Broadly Accessible 3D In Vitro Skin Model as a Comprehensive Platform for Antibacterial Therapy Screening

ACS APPLIED MATERIALS & INTERFACES

www.acsami.org
Research Article

Broadly Accessible 3D *In Vitro* Skin Model as a Comprehensive Platform for Antibacterial Therapy Screening

Simona Villata, Désirée Baruffaldi, Raquel Cue Lopez, Camilla Paoletti, Paula Bosch, Lucia Napione, Andrea M. Giovannozzi, Candido Fabrizio Pirri, Enrique Martinez-Campos, and Francesca Frascella*

Cite This: *ACS Appl. Mater. Interfaces* 2024, 16, 70284−70296

ABSTRACT: Skin infections are currently a worldwide emergency as antibiotic-resistant bacteria are spreading, leading to the ineffectiveness of most antibiotics and antibacterial strategies. Consequently, there is an urgency of developing and testing innovative antibacterial therapies. As traditional 2D cell culture and planktonic bacteria culture can be obsolete due to their incapability of resembling the complex infection environment, 3D *in vitro* skin models can be a powerful tool to test and validate therapies. In this article, a 3D *in vitro* epidermis−dermis skin model has been developed and biofabricated to be broadly available, reaching a balance between the simplicity and reproducibility of the model and its complexity in terms of wound, infection, and treatment response. The results are really promising, as the skin model developed a comprehensive physical barrier. To further investigate the skin model, controlled wounding, infection, and antibiotic treatments were performed. The results were remarkable: Not only was the unwounded epidermal barrier able to partially stop the bacterial proliferation, but the entire system reacted to both wound and infection in a complex and complete way. Extracellular matrix deposition and remodeling, inflammatory response, antimicrobial peptide production, and change in cellular behaviors, from epithelial to mesenchymal and from fibroblasts to myofibroblasts, were witnessed, with different extents depending on the bacterial strain. In addition, the inflammatory response to the antibiotic administration was opposite for the two bacterial infections, probably revealing the release of inflammatory endotoxins during *Escherichia coli* death. In conclusion, the presented 3D *in vitro* skin model has all the characteristics to be a future landmark as a platform for antibacterial strategy therapy testing.

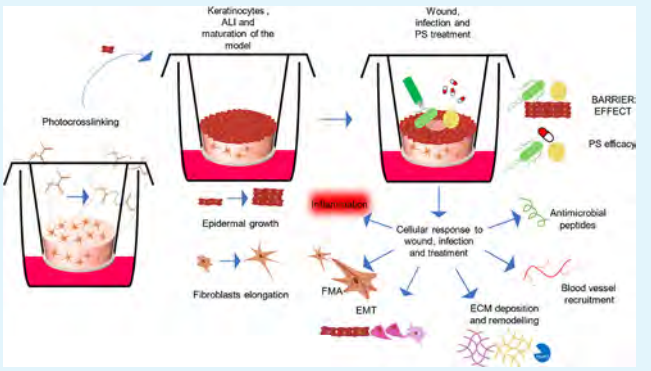

KEYWORDS: *3D in vitro skin model, barrier effect, wound healing, bacterial infection, immune response, therapy testing*

INTRODUCTION

Skin is the largest organ in the human body, and it is the main barrier between the latter and the external environment, protecting us from pathogen threats and maintaining overall health and homeostasis.[1] 3D *in vitro* models are for sure fundamental in drug testing and therapy screening, and they are replacing conventional 2D cell culture and animal models.[2] One of their main advantages is that they can replicate 3D organization and physiological functions of specific tissues at a relatively low cost, and they are usually easier to manage compared to animal models.[3,4] Development of a 3D *in vitro* model that accurately resembles the barrier function of human skin is crucial.[1] However, creating such a model that can be clinically translated comes with several challenges. Indeed, from the clinical point of view, 3D *in vitro* skin models based on human cells offer a more realistic platform for drug testing. As said, they reduce reliance on animal models and provide a better reflection of human skin responses. However, limitations still have to be overcome, including their inability to fully mimic the complexity of real skin, such as vascularization, immune interactions, and long-term healing processes, hindering their direct translation to clinical practice.[5] Also, human skin is a complex and heterogeneous tissue composed of multiple layers, each of them with distinct cellular components and structural characteristics.[6,7] Indeed, three main layers can be highlighted: epidermis, dermis, and hypodermis. The external one (i.e., epidermis) consists mainly of keratinocytes that, producing keratin, contribute to the skin's strength and resilience maintaining structural integrity and supporting cellular interactions, crucial for barrier function.[8] Going deeper, the following layer is dermis, mainly

Received: September 24, 2024
Revised: November 18, 2024
Accepted: November 21, 2024
Published: December 12, 2024

composed of fibroblasts that produce collagen, fibronectin, and other extracellular matrix components, which together provide strength, elasticity, and support to the other layers.[9] The deepest part of the skin is the hypodermis, constituted by adipose tissue, especially serving as an insulation layer.[10]

Many works have underlined the importance of dermis−epidermis interaction in building the skin barrier: fibroblasts interact with the epidermis to enhance its integrity and function, producing an extracellular matrix to provide structural support and secreting growth factors and cytokines to regulate epidermal cell proliferation, differentiation, and wound healing processes.[11,12] Another crucial role lies in its provision of structural elasticity, thanks to collagen type I deposition by regulating dermal fibroblasts, which, in turn, regulates mechanical cues, cell morphology, and cell activity.[13,14]

Given the importance of physical constraints and of the external microenvironment in tissue function maintenance, the *in vitro* models used to speed up our knowledge of the tissue must encompass the extracellular components. For that reason, in the past decade, many hydrogels from natural sources or chemical synthesis have been designed to reflect skin matrix properties. Among them, gelatin methacryloyl (GelMA), which is obtained from methacrylation of gelatin (i.e., denaturated collagen), represents a promising supporting matrix for *in vitro* cell culture across various biomedical applications, including skin.[2,15] Its key attributes include outstanding biocompatibility, biodegradability, and printability.[16,17] Additionally, the synthetic nature of GelMA allows the tunability of final hydrogel chemical and mechanical properties, due to its possibility of modulating the gelatin concentration and its degree of methacrylation.[16,18,19]

The present work proposed a GelMA-based 3D *in vitro* skin model, composed of both a dermal component (human fibroblasts embedded in the hydrogel) and a self-assembled epidermis (human keratinocytes), which reached complete differentiation resembling both the histological and molecular features of physiological skin, making it suitable for next functional tests.

As mentioned, skin infections are a common medical condition that can affect people of all ages and backgrounds[20,21] and are caused by harmful bacteria that disrupt the skin's normal functioning.[20] In general, the most dominant pathogen is *Staphylococcus aureus* (39.28%), followed by *Pseudomonas aeruginosa* (19.64%), *Escherichia coli* (30.35%), and *Enterococcus* spp. (10.71%).[22,23] Moreover, *Staphylococcus aureus/Escherichia coli* is a really common bacterial association that can be found in infected wounds.[24] Skin infections can vary in severity, but nowadays, the world has to face the significant challenge of antibiotic-resistant bacteria,[25−27] which have developed the ability to withstand the effects of antibiotics, making infections harder to treat[28] and leading to the necessity to develop new and alternative therapies.[27−29] For this reason, new *in vitro* platforms have been designed and optimized.[28,30] Existing literature presents efforts in development of functional *in vitro* infected skin models to test new antibacterial strategies;[31−33] however, there still are deficiencies. First, existing models often lack both the complexity (i.e., interaction between dermis and epidermis) and the 3D structure of the dermal compartment needed for a comprehensive understanding.[31,33] Furthermore, barrier efficiency is not tested or maintained during experiment, causing sample disruption after maximum 48 h of infection,[32,33] decreasing the power of the model. Finally, the lack of a systematic analysis of *in vitro* skin responses, in terms of both cellular behavior and signaling, to the wound, the pathogens, and the treatments decreased the understanding of the physiological response that influence also drug response.[34,35]

To fill these gaps, the GelMA-based 3D *in vitro* skin model, fully characterized before the infection, has been wounded and infected with two different bacterial strains: *Staphylococcus aureus* (*S. aureus*, Gram-positive) and *Escherichia coli* (*E. coli*, Gram-negative).[22,23] Finally, to validate the infected model, penicillin−streptomycin (PS) was chosen as treatment, being a well-known and broad-spectrum antibiotic, conventionally used also during the culture of various kinds of cell lines.[36,37] Both the antibacterial efficacy of PS and the skin response in terms of RNA expression were analyzed, to be able to completely characterize the model response. Once again, the response of both the bacteria and the skin model was physiological and promising in a frame of standardization purpose.

In conclusion, what has been obtained is the development of a dermis−epidermis 3D *in vitro* skin model that can be used as a platform to test new and alternative therapies against wound infections. Its simplicity but precision in resembling the *in vivo* skin barrier places it in a leading position, with the perspective of standardizing antimicrobial testing procedures, making them accessible to as many laboratories as possible.

1. MATERIALS AND METHODS

1.1. GelMA Synthesis. GelMA was produced according to Van Den Bulcke et al.[38] In summary, 10 g of type B gelatin sourced from bovine skin (Sigma-Aldrich, 225 Bloom) was dissolved in Dulbecco's phosphate-buffered saline (DPBS, Sigma) at a concentration of 10% w/v and heated at 50 °C for 1 h. To introduce methacrylate groups to gelatin's reactive amine and hydroxyl groups, 8 mL of methacrylic anhydride (MAA, Sigma-Aldrich) was gradually incorporated. The reaction lasted for 2 h at 40 °C under magnetic stirring before being interrupted by dilution with an equal volume of DPBS. The resulting solution underwent a 2-week-long dialysis process against double-distilled water (dd-H_2O) using a cellulose membrane with a molecular weight cutoff of 12−14 kDa (Sigma-Aldrich) at 40 °C, aimed at eliminating any remaining unreacted MAA. Finally, GelMA was subjected to freeze-drying and stored for further use.

1.2. Skin Model. GelMA formulation for dermis recapitulation was obtained by dissolving the synthesized GelMA at 10% w/v concentration in DMEM (Gibco) cell culture medium, previously combined with lithium phenyl-2,4,6-trimethylbenzoylphosphinate (LAP) as a photoinitiator at a concentration of 2.5 mg/mL. The solutions were heated at 60 °C for 1 h and filtered through 0.22 μm PES membrane filters (Asimo) to sterilize. GelMA solution was prewarmed at 37 °C before cells were added.

Once GelMA solution was obtained, human fibroblasts (HFF-1, Atcc) were encapsulated in the hydrogel at a concentration of 1.5 × 10^6 cells/mL and carefully dispersed, and then 300 μL of HFF-1-laden GelMA was seeded on PET 12-well hanging inserts, with a porosity of 0.4 μm (Millicell). To stabilize the dermis layer, constructs were photo-cross-linked thanks to UV-light irradiation ((λ = 365 nm, Asiga Flash Cure Box, I = 10 mW cm^{-2}) for 1 min. Once the stable dermis layer was obtained, human keratinocytes (HaCaT, Antibody Research Corporation) were seeded on top of the dermis, using 2 × 10^5 cells/insert. The first 3 days of culture were performed as submerged culture, in complete DMEM (15% FBS, 2% L-glutamine, 1% penicillin−streptomycin, and 1% sodium pyruvate). Specifically, this involved using 1.5 mL of medium in the lower compartment and 1 mL in the upper compartment. This phase was necessary to facilitate the adhesion of keratinocytes to the upper portion of the dermis. After the first 3 days, air−liquid interface (ALI) culture started, supplying 500 μL of 3dGRO Skin Differentiation Medium (Sigma) in the lower

https://doi.org/10.1021/acsami.4c16397
ACS Appl. Mater. Interfaces 2024, 16, 70284−70296

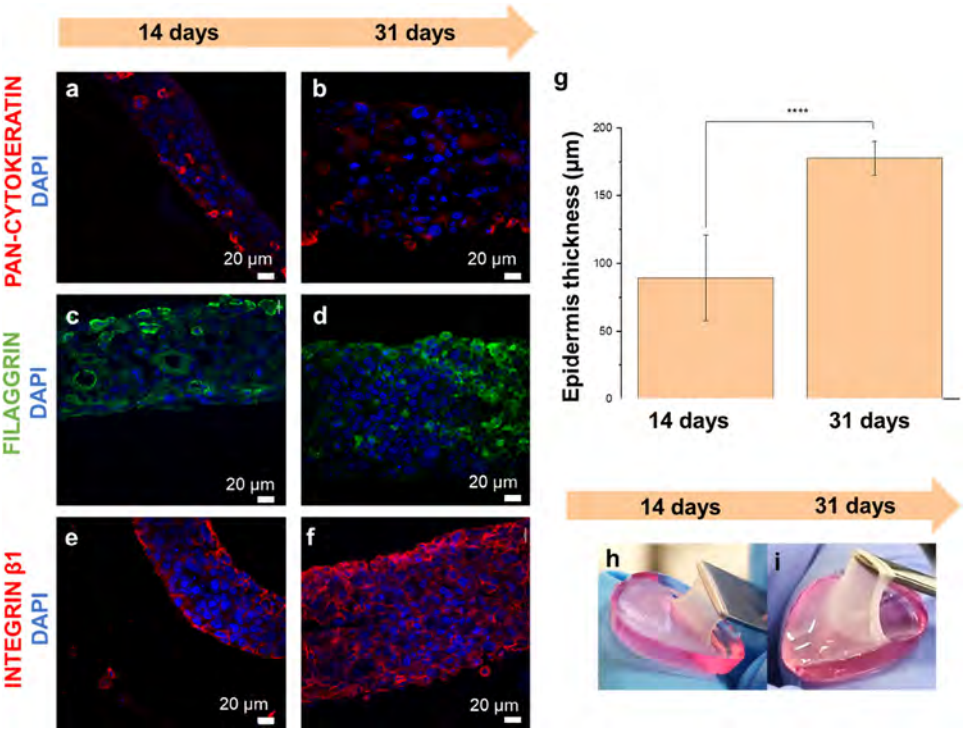

Figure 1. Immunofluorescence images of pan-cytokeratin (red) expression after 14 (a) and 31 (b) days of culture, filaggrin (green) expression after 14 (c) and 31 (d) days of culture, and CD29 (red) expression after 14 (e) and 31 (f) days of culture. Cells nuclei are stained in blue (DAPI). Epidermis thickness evaluation from immunofluorescence images. (g) Pictures of epidermis mechanical detachment from dermis to visualize the epidermal compartment after 14 (h) and 31 (i) days of culture. Statistical analysis was performed with one-way ANOVA (*$p < 0.05$, **$p < 0.01$, ***$p < 0.001$, ****$p < 0.0001$).

compartment and leaving the upper compartment in contact with air. Culture proceeded for a total of 14 or 31 days, and medium was changed every 2 days.

1.3. Skin Characterization. *1.3.1. Immunofluorescence.* Skin models were stained after 14 and 31 days of culture. Specifically, the samples were fixed in paraformaldehyde 4 v/v% in DPBS (J61899.AK, Thermo Scientific) for 1 h at RT. After three washing steps in DPBS (10 min at RT), some samples were permeabilized with 0.25 v/v % of Triton X-100 (Sigma-Aldrich) for 15 min incubated with 1 μM DAPI in DPBS and 0.25 μM FITC-conjugated phalloidin in PBS for 1.5 h at room temperature. To obtain sliced samples, other fixed samples were incubated for 1 h in 30 w/v% sucrose solution and then included into PolyFreeze Tissue Freezing Media (SHH0026, Sigma-Aldrich) and frozen at −80 °C. The samples were sliced on cryotome to create 40 μm-thick sections, mounted on glass slides, and kept at −80 °C. For staining, the sections were washed in DPBS, permeabilized with 0.1 v/v % of Triton X-100 (Sigma-Aldrich) for 10 min, and blocked with a solution of 5 w/v% BSA (Sigma-Aldrich) and 0.1 v/v% Tween (Sigma-Aldrich) for 1 h. For the skin model analysis, three different antibodies were used at specific dilution: pancytockeratin (2 μg/mL, NovusBio), CD29 (integrin β1) (2 μg/mL, Invitrogen), and filaggrin (10 μg/mL, Invitrogen). Bacteria were stained with *S. aureus* antibody (50 μg/mL, 0300-0084 Bio-Rad) and *E. coli* antibody (200 μg/mL, 4329−4916 Bio-Rad). Specifically, primary antibodies were incubated overnight at 4 °C, and after three washing steps in DPBS supplemented with 0.1 vol % Tween, the staining with appropriate secondary antibodies (Invitrogen, 1:1000 from mother solution) lasted 1 h at RT. Nuclei were stained with 1 μM DAPI solution for 30 min and (if needed) with 11 μM Alexa Fluor Plus 555 phalloidin (Invitrogen) in PBS. At the end, the samples were mounted with Mowiol (Sigma-Aldrich) and then analyzed by using a microscope (ECLIPSE Ti2 Nikon, Tokyo, Japan) equipped with a Crest X-Light spinning disk confocal microscope. Image analysis was performed with ImageJ software.

1.3.2. Live and Dead. The LIVE/DEAD cell assay kit (Sigma-Aldrich) was used to evaluate cell viability and to obtain morphological information after 14 and 31 days of culture. In detail, skin samples were washed twice with DPBS, stained with 1.5 μM propidium iodide (PI) and 1 μM Calcein-AM for 30 min in an incubator at 37 °C, and washed again with DPBS to remove the unreacted dyes. The fluorescence signals were detected using an Eclipse Ti2 Nikon microscope equipped with a Crest X-Light spinning disk.

1.4. PS Screening on Bacteria. Cultures of *S. aureus* subsp. aureus Rosenbach (ATCC 25293 or ATCC 6538P) and *E. coli* (Migula) Castellani and Chalmers (ATCC 10536 or ATCC 8739) bacteria that had been allowed to grow in Luria−Bertani broth (Thermo Fisher) overnight (37 °C and 125 rpm) were adjusted to an optical density (OD) of 1.0 at 600 nm. Subsequently, they were diluted at a 1:10 ratio in treatment solution when the experiment started. 5 mL of 1:10 bacterial suspension (for both bacterial strains) was incubated for 24 h in a solution of Luria−Bertani broth and penicillin−streptomycin (PS, Thermo Fischer Scientific, 10,000 units/mL penicillin and 10,000 μg/mL streptomycin) at 2, 5, 10, or 20% v/v (37 °C, 125 rpm). The control group consisted of Luria−Bertani broth without PS. After a 24 h incubation period, the remaining viable bacteria resulting from PS treatment were revealed measuring the OD at 600 nm.

1.5. PS Screening on 2D Human Cells. HaCaT and HFF-1 cells were cultured in complete DMEM (15% FBS, 2% L-glutamine, 1% penicillin−streptomycin, and 1% sodium pyruvate). Cell cultures were maintained at 37 °C in a humidified incubator with 5% CO_2. Cells were initially seeded at a density of 1×10^4 cells/well into a 96-well cell culture plate (200 μL of complete DMEM for each well) and incubated at 37 °C for 24 h. After 24 h, the cell culture medium was removed, and 200 μL of penicillin−streptomycin (PS) at concentrations of 2, 5, 10, or 20% v/v in complete DMEM was added to cells. To assess the metabolic activity of cells exposed to PS after 24 h of treatment, PrestoBlue metabolic assay was employed. PrestoBlue

https://doi.org/10.1021/acsami.4c16397
ACS Appl. Mater. Interfaces 2024, 16, 70284−70296

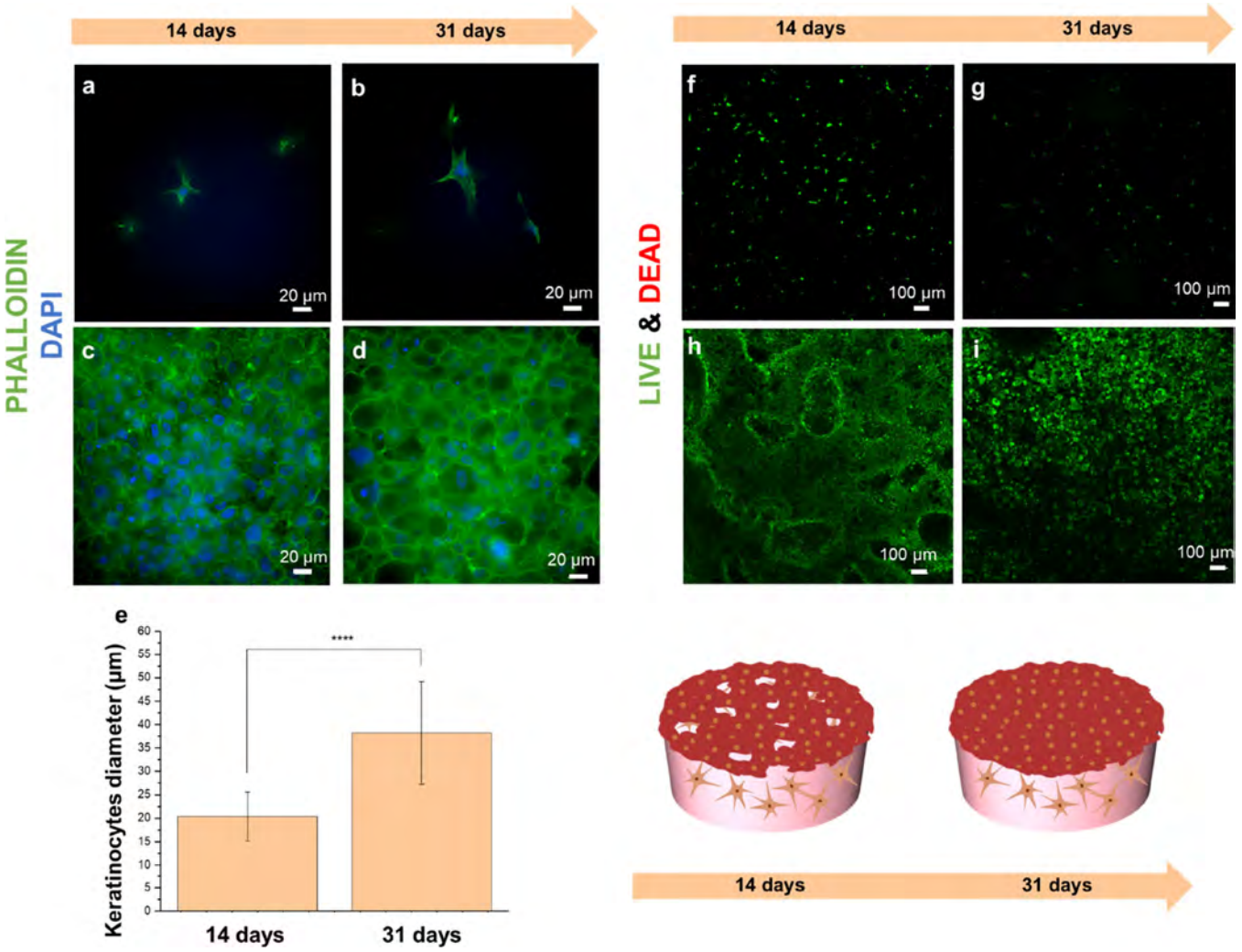

Figure 2. DAPI−phalloidin staining of both dermis (a 14 days, b 31 days) and epidermis (c 14 days, d 31 days); scale bar is 20 μm. Difference in keratinocyte diameter in the outer layer of the epidermis after 14 and 31 days of culture (e). Live and dead assay of both dermis (f 14 days, g 31 days) and epidermis (h 14 days, i 31 days); scale bar is 100 μm. Statistical analysis was performed with one-way ANOVA (*$p < 0.05$, **$p < 0.01$, ***$p < 0.001$, ****$p < 0.0001$).

(Sigma-Aldrich, UK) was diluted in complete DMEM 1:10, replaced to the DMEM−PS mixture, and incubated for 90 min before fluorescence measurements were taken (exc/em: 530/590). The control group consisted of complete DMEM without PS.

1.7. Skin Model Infection and Treatment. Skin models were cultured for 31 days before starting the bacterial infection. Prior to the infection, some skin models were wounded with a 3 mm-diameter biopsy surgical punch to interrupt the epidermal barrier and to see the difference in infection spread between wounded and unwounded skin. To perform the infection, 10 μL of *S. aureus* or *E. coli* at OD 1.0 in Luria−Bertani broth was inoculated inside the wound or in the center of the epidermis (in case of unwounded skin). The infection was left spread for 24 h, and then 100 μL of PS 5% in DPBS was poured on top of the epidermis. After the other 24 h (the treatment time), the samples were homogenized in 900 μL of DPBS and serial dilutions were made before seeding on agar plates. The next day, colony-forming unit (CFU) counting was performed to assess the extent of bacterial growth. Skin models were also prepared for immunofluorescence (Section 2.1) or for the droplet digital-polymerase chain reaction (Section 2.4).

1.8. RNA Extraction and Droplet Digital-Polymerase Chain Reaction (ddPCR). For total RNA extraction, cells were retrieved from GelMA. The hydrogels were digested with 0.5 mg mL^{-1} collagenase (C9407, cod. Sigma-Aldrich) in DMEM for 2 h at 37 °C and then centrifuged at 1200 rpm for 5 min to pellet the cells. The harvested cells were put in 1 mL of TRIzol Reagent (cod. 15596026, Invitrogen). The RNA was derived following the manufacturer's instruction; in particular, 200 μL of chloroform (Sigma-Aldrich) was added to the solution and mixed. Then, the solution was centrifuged at 12,600 rpm for 30 min and the derived aqueous phase was transferred into a new tube. The RNA was precipitated overnight at −20 °C by adding 500 μL of isopropanol (Sigma-Aldrich). The next day, samples were centrifuged for 30 min at 12,600 rpm and the pellets were washed twice with 1 mL of 70 v/v% of ethanol at 7400 rpm for 15 min. At the end, pellets were dried under a chemical hood and resuspended in 40 μL of nuclease-free water. The RNA concentration was determined by using Synergy HTX Multi-Mode Microplate Reader (BioTek, Winooski, Vermont, USA). Reverse transcription of 250 ng of RNA into cDNA was performed using a High-Quality cDNA Reverse Transcription kit (cod. 4368814, Applied Biosystems, USA), according to the manufacturer's protocol. ddPCR was performed to assess the expression of COL1A1 (ID assay: dHsaCPE5034391), FN1 (ID assay: dHsaCPE5035056), ACTA2 (ID assay: dHsaCPE5051320), CDH1 (ID assay: dHsaCPE5032390), CDH2 (ID assay: dHsaCPE5052923), MMP2 (ID assay: dHsaCPE5033158), TP53 (ID assay: dHsaCPE5037520), VEGFA (ID assay: dHsaCPE5034757), IL-6 (ID assay: dHsaCPE5036918), IL-1A (ID assay: dHsaCPE5054237), IL-8 (ID assay: dHsaCPE5040425), TNF (ID assay: dHsaCPE5190841), and DEFB103B (ID assay: dHsaCPE5190417) using ddPCR Supermix

https://doi.org/10.1021/acsami.4c16397
ACS Appl. Mater. Interfaces 2024, 16, 70284−70296

for probes without dUTP. Droplet generation was performed according to the manufacturer's instructions. Thermal-cycling conditions were 95 °C for 10 min (1 cycle), 94 °C for 30 s and 55 °C for 30 s (40 cycles), 98 °C for 10 min (1 cycle), and a 4 °C infinite hold. In all ddPCR experiments, the PCR plate was loaded on a Bio-Rad QX200 droplet reader for quantification of cDNA copies/μL. Analysis of the ddPCR data was performed by Bio-Rad QuantaSoft software. GAPDH (ID assay: dHsaC-PE5031597) was used as a housekeeping gene to perform quantitative normalization. Results were reported as the concentration (cDNA copies μL^{-1}) of the gene of interest with respect to the mean concentration (cDNA copies μL^{-1}) of GAPDH.

1.9. Statistical Analysis. For the statistical analysis of epidermis thickness (Figure 1i) and keratinocyte diameter (Figure 2i), one-way ANOVA (analysis of variance) was used to determine the mean and standard deviation. Two-way ANOVA was used for the CFU evaluation in Figure 4e,f. ANOVA also generated a p-value. In all graphs, significance levels are indicated: *$p < 0.05$; **$p < 0.01$; ***$p < 0.001$; ****$p < 0.0001$.

For ddPCR analysis (Figures 5, 6, and 7), unpaired t test was employed, and in all the graphs, the significance level was $p < 0.05$.

3. RESULTS AND DISCUSSION

2.1. Skin Model Establishment and Characterization.

2.1.1. Epidermal Development. At the beginning of this study, the evolution of epidermis formation over 31 days of culture to confirm the correct differentiation of the cells was investigated. For this reason, skin specimens were stained with epidermal markers, i.e., pan-cytokeratin, filaggrin, and CD29 (integrin β1). All of them are involved in the formation of organized, stable, and functional barriers, which are fundamental for the establishment of reliable skin models.

Specifically, cytokeratins are a group of proteins that constitute intermediate filaments and primary cytoskeletal components that provide structural support to keratinocytes.[39] As expected in healthy keratinocytes, their expression, detected by pan-cytokeratin antibody, was found both after 14 (Figure 1a) and 31 days (Figure 1b), confirming the survival and growth of the upper layer of the model. Then, the focus moved on filaggrin, a structural protein mainly found in the outermost layer of the epidermis, known as the stratum corneum (SC). It is responsible for generating natural moisturizing factors that contribute to barrier functions by protecting skin against microbial colonization, and for assembling keratin filaments, leading to the creation of a network that leads to the transformation of keratinocytes into flattened corneocytes.[1,40] Relevantly, reduced filaggrin expression resulted in increased epidermal bacterial colonization.[41] As for pan-cytokeratin, filaggrin expression was found after both 14 (Figure 1c) and 31 days (Figure 1d), demonstrating the formation of a functional layer able to act as a protective barrier. To conclude this preliminary characterization, the potential of the formed epidermis to adhere beneath the matrix was investigated by detecting high integrin β1 (CD29) expression (Figure 1e,f). Within keratinocytes, CD29 serves the dual function of facilitating the attachment to the extracellular matrix and governing the initiation of terminal differentiation.[42]

This investigation also demonstrated the evolution of the epidermis over the culture, showing the higher thickness after 31 days (Figure 1g), suggesting the formation of a thicker barrier against the external environment.[43] The epidermal compartment after 31 days was 178 ± 12 μm thick, which is in line with *in vivo* human epidermal thickness.[44,45] The dermal thickness, instead, was obtained during the biofabrication process, once again in line with *in vivo* human dermis thickness.[45]

The thickening of the epidermis was also macroscopically perceptible in Figure 1h,i, underlying the idea that the skin model develops a stronger barrier after 31 days of culture.

2.1.2. Cellular Viability and Morphology. Bulk samples (i.e., not sliced) were fixed and stained with both DAPI- and FITC-conjugated phalloidin to analyze the change of cellular shape through culture time. In Figure 2a,b, it is possible to notice the differences in fibroblast shape, as after 31 days they appeared more elongated, underlying a stronger interaction with the matrix they are embedded into.[14] From the epidermis point of view (Figure 2c,d), the outer layer of the skin model presented a change in morphology. Keratinocytes, found smaller and more defined after 14 days, were bigger in terms of planar diameter after 31 days (Figure 2e) and both borders between cells and cellular nuclei were less defined. These features suggest the progressive cornification of the epidermal compartment.

To obtain a qualitative analysis of the cell viability, a live and dead assay was performed on the dermal (Figure 2f,g) and epidermal (Figure 2h,i) compartments, after 14 (Figure 2f,h) and 31 (Figure 2g,i) days of culture. The vitality was in every case higher than 95%, underlying GelMA as a great environment for cellular culture, and this, together with the fibroblasts' ability to elongate (DAPI−phalloidin staining in Figure 2a,b) after 31 days, hinted a stronger interaction with the matrix they were embedded into.[14] From the epidermis point of view, apart from a change in keratinocyte shape (DAPI−phalloidin immunofluorescence, Figure 2c,d), it was possible to also notice a more compact external epidermal layer, whereas after 14 days, the epidermis showed holes in the outer layers. That was further evidence that 31 days were necessary to have a better developed model.

High viability, fibroblast elongation, and epidermis homogeneity indicated that the design protocol allowed the obtaining of a fully mature model after 31 days of culture, the period after which functional tests could be carried on, considering the results based on a reliable model.

2.2. PS Condition Screening. Once the skin model was validated, the study moved on to the introduction of the bacterial stimuli to test the efficiency of the *in vitro* culture to resemble physiological response and antibiotic efficacy. Especially for the latter part, it was essential to subject the model to a standard antibiotic treatment to test its potential future utilization as a novel platform for the study of new and alternative therapies, establishing it as a benchmark. PS was selected as it is commonly used to prevent bacterial contamination of cell cultures due to its effective combined action against Gram-positive and Gram-negative bacteria. What must be taken into consideration is that the antibacterial compound has to be effective against bacteria but not harmful against cells. For this reason, four different PS concentrations (i.e., 2, 5, 10, and 20%) were tested both on planktonic bacteria (*S. aureus* Figure S1a and *E. coli* Figure S1b) and on 2D cell cultures (HaCaT Figure S1c and HFF-1 Figure S1d). Based on the findings, it can be inferred that the most favorable condition was the treatment with a 5% concentration of PS. This concentration effectively eradicated bacteria while ensuring a high survival rate of cells, significantly in the case of HFF-1 cells, which exhibited higher susceptibility at PS concentration of 10 and 20%.

https://doi.org/10.1021/acsami.4c16397
ACS Appl. Mater. Interfaces 2024, 16, 70284−70296

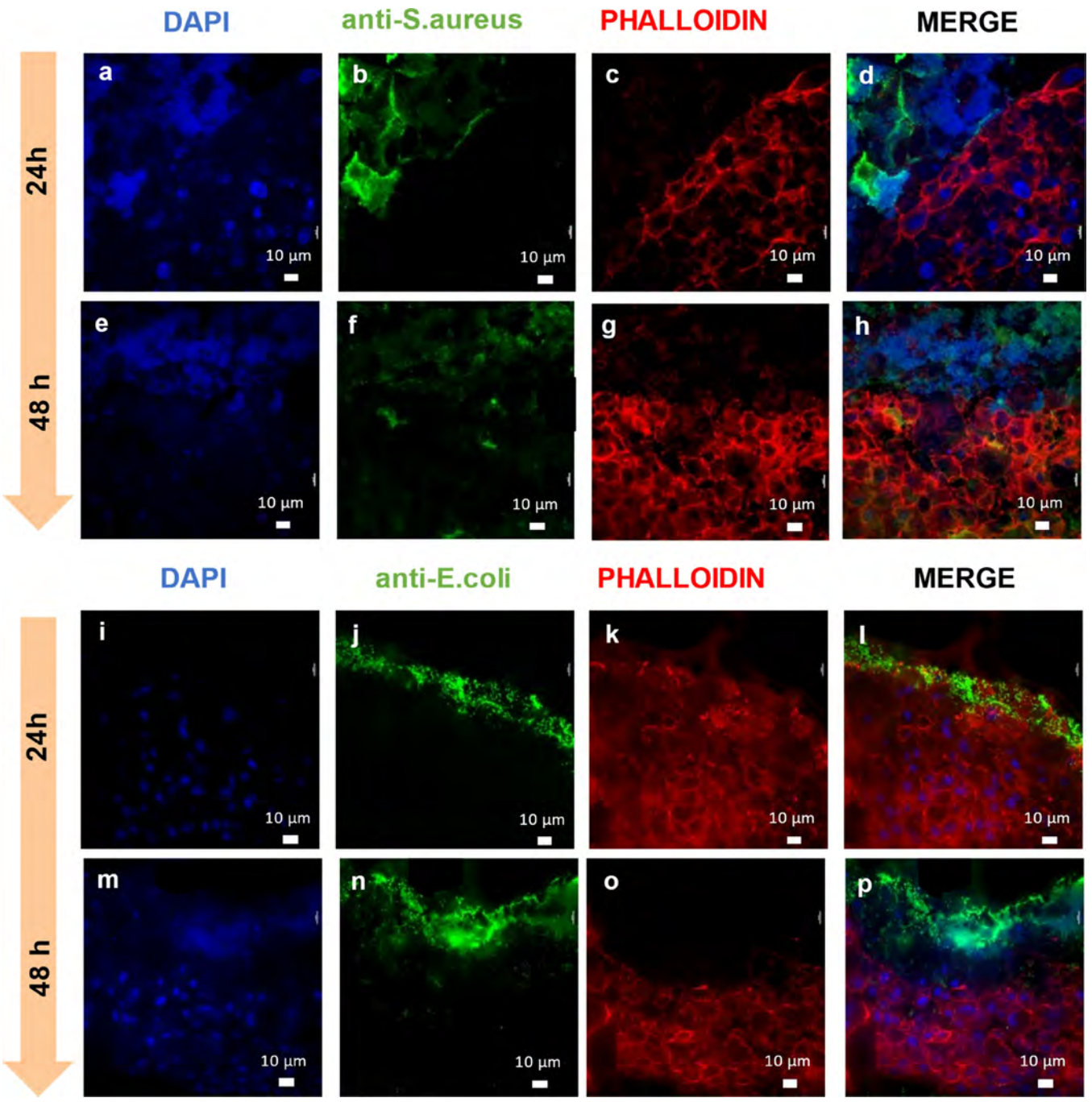

Figure 3. Immunofluorescence images of the 3D *in vitro* skin model inoculated with both *S. aureus* (a–h) and *E. coli* (i–p). Analysis was performed 24 h (a–d, i–l) and 48 h (e–h, m–p) after the bacterial inoculation. DAPI was used to stain both bacteria and cell nuclei (a, e, i, m); TRITC–phalloidin stained the cytoskeletons of cells (c, g, k, o), and in the FITC channel, it is possible to observe both bacterial strains (b, f, j, n).

2.4. Skin Model Bacterial Infection and Treatment. *2.4.1. Bacterial Penetration into the 3D Skin Model.* To visualize the ability of both *S. aureus* (Figure 3a–h) and *E. coli* (Figure 3i–p) to penetrate the 3D skin model, after 31 days of maturation, *S. aureus* or *E. coli* was inoculated in the center of the epidermal compartment. Samples were fixed, sliced, and stained both after 24 h (Figure 3a–d,i–l) and 48 h (Figure 3e–h,m–p). The results highlighted the role of the epidermal barrier role in blocking these two pathogens. Observational information from the pictures indicated that both bacterial strains grew over time, but the epidermis remained intact, preventing the invasion by bacteria of the dermis underneath, protecting it from external threats.

2.4.2. Bacterial Infection and Treatment. To perform the infection, a 31-day-old skin model was subjected to wounding and bacterial inoculation, as described in Section 1. In Figure 4a, it is possible to visualize the unwounded model, just before the start of the experiment. Figure 4b shows the sample once the wound is performed, and Figure 4c and 4d shows the skin sample after 24 or 48 h of infection, respectively. CFU counting results are reported in Figure 4e for *S. aureus* and Figure 4f for *E. coli*. The results were similar between the two bacterial strains: when PS treatment was not administered, the

https://doi.org/10.1021/acsami.4c16397
ACS Appl. Mater. Interfaces 2024, 16, 70284–70296

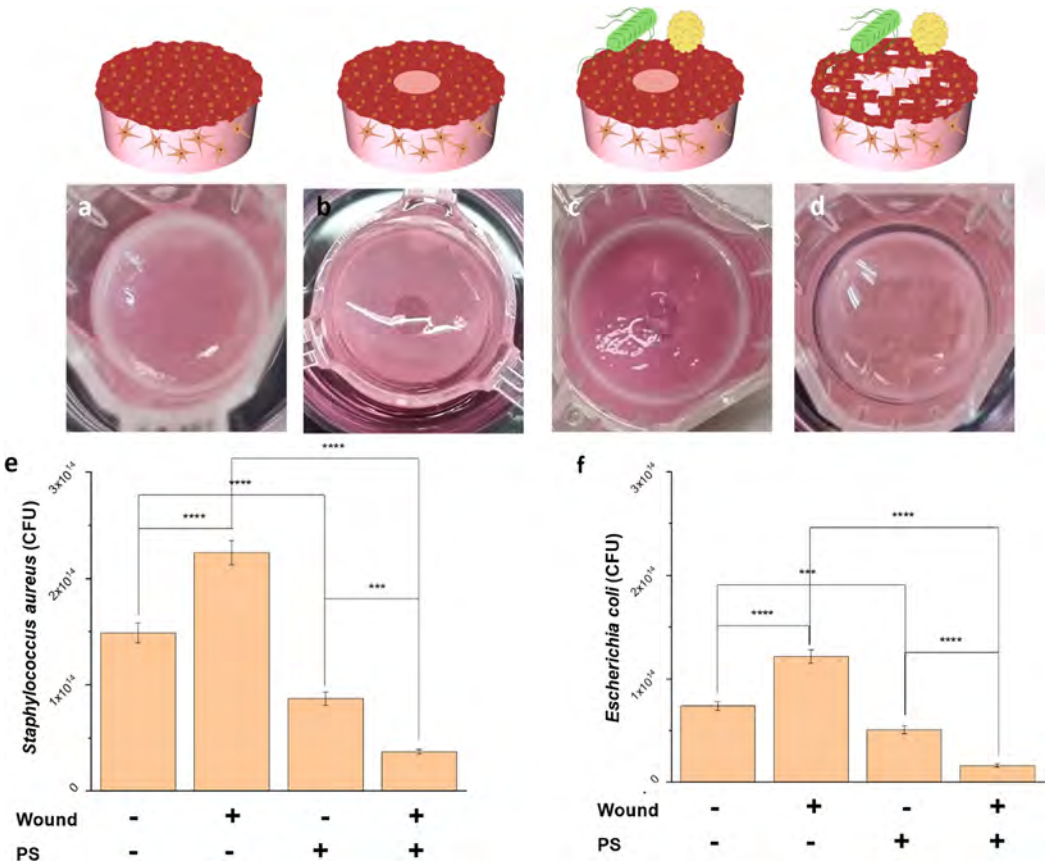

Figure 4. Pictures of skin models unwounded (a), once the wound is performed (b), and after 24 h (c) or 48 h (d) of infection. CFU counting of *S. aureus* (e) and *E. coli* (f) after 48 h of infection, with or without a wound and with or without PS treatment. Statistical analysis was performed with two-ways ANOVA (*$p < 0.05$, **$p < 0.01$, ***$p < 0.001$, ****$p < 0.0001$).

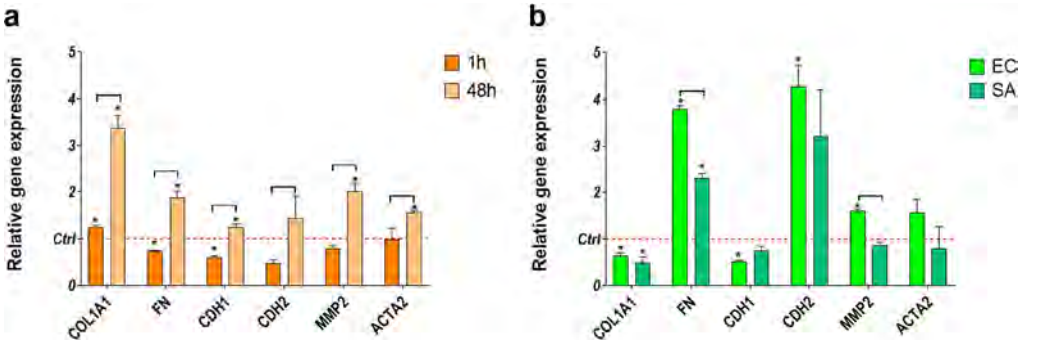

Figure 5. Modulation of cellular behavior in response to wound and bacterial infection. (a) Gene expression analysis of wounded samples after 1 h (dark orange) and 48 h (light orange). The results are shown as fold change ± SD on the respective non-wounded control (Ctrl: red dotted line). (b) Gene expression analysis of wound samples after 48 h of exposure to bacterial infection by *E. coli* (EC, light green) or *S. aureus* (SA, dark green). The results are shown as fold change ± SD on the signal of the noninfected wound (Ctrl: red dotted line). In both graphs, statistical significant differences are shown by black line above the bar (1 vs 48 h) or by a star (sample vs ctrl).

spread of infection was more extensive, especially in the wounded samples, confirming again the protective role of the epidermal barrier in preventing bacterial infection expansion. However, when PS treatment was applied, a contrasting pattern emerged, with a higher level of infection detected in the unwounded models and a lower level in the wounded ones, highlighting, once again, the barrier efficacy of the model that was effective not only for bacterial infection but also for drug penetration.

2.4.3. Droplet Digital PCR. Modulation of Cellular Behavior in Response to Wound and Bacterial Infection. To investigate how the wound trauma influences cellular behavior (Figure 5a), RNA from skin samples was extracted and analyzed through ddPCR. Analyzing the selected genes, it was possible to witness a general activation of the model: after 48 h, the expression of FN1 (fibronectin), COL1A1 (collagen type I), and MMP2 (matrix metalloproteinase 2) was enhanced, and at the same time, ACTA2 (α-SMA) was upregulated. Fibronectin has been witnessed to have roles in all the wound healing phases,[46,47] but in early stages, there is the production of plasma fibronectin, from hepatocytes, and only later tissue fibronectin is produced, mostly by fibroblast (but

https://doi.org/10.1021/acsami.4c16397
ACS Appl. Mater. Interfaces 2024, 16, 70284−70296

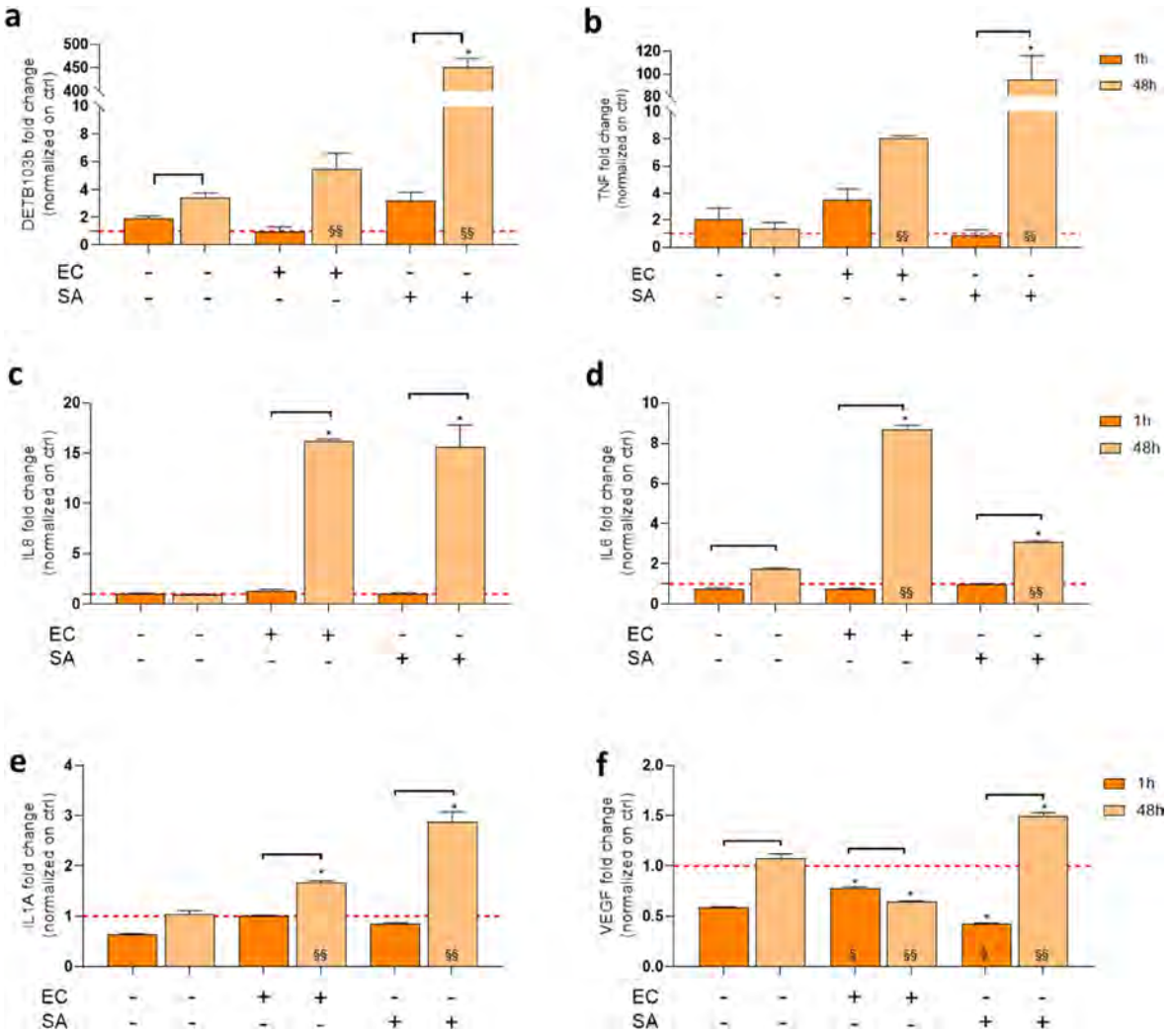

Figure 6. Gene expression analysis of wounded samples after 1 or 48 h of exposure or not to bacterial infection by *E. coli* (EC) or *S. aureus* (SA). Analyzed genes have been (a) DETB103b, (b) TNF, (c) IL-8, (d) IL-6, (e) IL-1A, and (f) VEGF. The results are shown as fold change ± SD on the signal of not wounded and not infected samples after 1 or 48 h, respectively (Ctrl: red dotted line). In both graphs, statistically significant differences are shown by a black line above the bar (1 vs 48 h) and by a star (sample vs ctrl). In the nonwound sample, the statistical differences between EC vs SA are indicated by # (1 h) and ## (48 h); in the wounded ones by § (1h) or §§ (48h).

also by keratinocytes[47]). Also, collagen type I (COL1A1) is a key component of the extracellular matrix; it is mostly produced by fibroblast and plays critical roles in the regulation of the phases of wound healing.[48] MMP2, on the contrary, is well known to contribute to remodeling during wound healing by breaking down different elements of the extracellular matrix.[49,50] They also promote cell spreading by degrading the nearby microenvironment, thus decreasing mechanical restrictions around cells.[49,50] Interestingly, some hypotheses have also been made on the presence of MMP-sensitive motifs in GelMA.[51] ACTA2 (responsible for the synthesis of α-SMA) upregulation witnessed the fibroblast activation into myofibroblasts (fibroblast−myofibroblast activation, FMA). Thus, it is well known that during wound healing, fibroblasts are activated into myofibroblasts that, thanks to elevated α-SMA (alpha smooth muscle actin) levels, can increase mechanical tension to induce a more rapid wound closure.[52] Thus, the wound presence was able to induce the remodeling of the environment (MMP2, COL1A1, and FN1) from one side and the activation of the fibroblasts into myofibroblasts (ACTA2) from the other side.

The subsequent infection was able to impair and modify the wound healing progression, as shown in Figure 5b. With both bacterial strains, the extracellular matrix production was biased toward fibronectin (FN1), resulting in the downregulation of COL1A1. The upregulation of FN1 was higher for *E. coli* infection. After a cutaneous injury, fibronectin is immediately released and deposited by cells, becoming a crucial ECM component.[53,54] Its fibrils form scaffolds for other ECM proteins, such as collagens.[53] As in the presence of bacteria there was an impairment in the regulation of FN1 and COL1A1, it is possible that the infected wound healing is moving through a fibrotic scenario. *E. coli* infection, moreover, enhanced the expression of MMP2, witnessing a higher effort in breaking down the extracellular matrix. Moving on, *E. coli* infection was able to activate the epithelial−mesenchymal transition (EMT). EMT is a physiological process occurring during cutaneous wound healing, during which stationary keratinocytes of the epidermis migrate across the wound bed to restore the epidermal barrier.[55,56] The crucial step for EMT is the loss of epithelial cell markers (CDH1, responsible for the synthesis of E-cadherin) and the gain of mesenchymal cell

https://doi.org/10.1021/acsami.4c16397
ACS Appl. Mater. Interfaces 2024, 16, 70284−70296

markers (CDH2, responsible for the synthesis of N-cadherin). The same trend of CDH1 downregulation and CDH2 upregulation was detected in *S. aureus* infection but was not statistically significant. It has to be noticed that EMT was only observed in response to infection but not with wounding alone. This suggests that the infection (in particular with *E. coli*) provided additional stress to the skin model that was necessary to trigger EMT, whereas simple wounding was not enough to activate this process. Interestingly, *in vivo*, wounding alone is enough to induce EMT, highlighting a potential limitation of the 3D *in vitro* skin model in fully recapitulating the wound healing response.[56] FMA was not impaired by bacterial infection, and it is important to underline that EMT and FMA can be connected, as these processes *in vivo* sometimes converge into what is known as epithelial-to-myofibroblast transition.[57] In this process, epithelial cells undergo EMT, transforming into mesenchymal-like cells, which can further and almost immediately differentiate into myofibroblasts. Interestingly, even if the difference was not statistically significant, *E. coli* infection, which significantly led to EMT, presented higher levels of ACTA2.

In Figure S2, the same genes for the infected but not wounded skin were reported. It is possible to observe that the presence of bacteria led to a modulation of the cellular behavior, but in a lower extent than the wounded counterpart, probably indicating a lower contact between cells and bacteria thanks to the epidermal barrier effect.

Modulation of Cellular Signaling in Response to Wound and Bacterial Infection. RNA quantification through dddPCR was also employed to investigate how wound trauma and subsequent infection influenced cellular signaling (Figure 6). DETB103b is the gene responsible for the synthesis of hBD-3 (i.e., human β-defensin 3, Figure 6a and Figure S3a), an antimicrobial peptide produced by resident keratinocytes.[58,59] Even if an upregulation trend was found after 48 h in an infected but unwounded skin model (Figure S3a), assessing a keratinocyte activity also if the epidermal barrier is intact, during the wound infection, the trend was opposite for the two bacteria: *E. coli* presence did not lead to an upregulation of the gene, while *S. aureus* did. This behavior was expected, as hBD-3 is specifically associated with *S. aureus* infection control.[60] To assess the inflammatory response of the 3D *in vitro* skin model, the expression of gene transcribing for four proinflammatory cytokines TNF (TNF-α, Figure 6b and Figure S3b), IL-8 (IL-8, Figure 6c and Figure S3c), IL-6 (IL-6, Figure 6d and Figure S3d), and IL-1A (IL-1a, Figure 6e and Figure S3e) was analyzed. These cytokines were selected as they all are involved in the immune response during skin infection: TNF-α is involved in the early process of wound healing,[61] IL-8 is a vital neutrophil chemotactic factor,[58] IL-1a is produced by keratinocytes to attract immune cells,[58] and IL-6 is essential for innate immune responses to bacteria and other microorganisms. It was one of the earliest fibroblast cytokines discovered, even if it is now also associated with keratinocytes.[62,63] While the wound alone was not able to induce a response in terms of cell signaling, bacterial presence increases the production of all the cytokines, in both unwounded (see the Supporting Information and Figure S3) and wounded samples, with different extents depending on the cytokine and the bacterial strain. Focusing on wounded samples, *E. coli* triggered an enhanced expression of IL-8, IL-6, and IL-1A (IL-6 was more expressed than in *S. aureus* infection). During *S. aureus* infection, the IL-1A-enhanced expression was higher than in *E. coli* infection and, moreover, also TNF was overexpressed. IL-8 was overexpressed in both infections, without significant differences between the bacterial strains. Finally, VEGF (responsible for the synthesis of VEGFA, Figure 6f and Figure S3f) upregulation can have many purposes: it can enhance vascular permeability, inflammation levels, and angiogenesis, but it is also involved in wound closure and re-epithelization and granulation tissue deposition.[64] While the wound alone did not enhance VEGF levels, the infection led to two different effects for the two bacterial strains: in *E. coli* infection, the VEGF was downregulated (low VEGF levels can contribute to impaired healing and the development of chronic, nonhealing wounds),[64] while in *S. aureus* infection, it was upregulated after 48 h, and high VEGF levels could promote overabundant scar tissue formation.[64]

Modulation of Cellular Signaling during PS Treatment. Finally, ddPCR was used to investigate how the PS treatment could influence cellular signaling (Figure 7). In noninfected

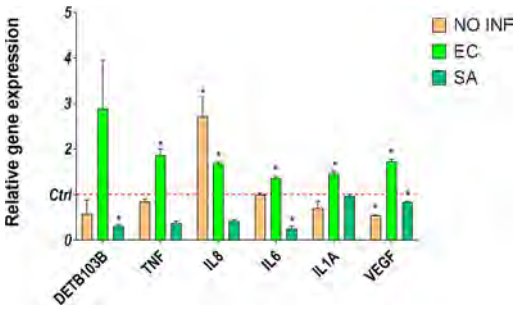

Figure 7. Gene expression analysis of wound samples after 48 h of exposure to bacterial infection by *E. coli* (EC, light green) or *S. aureus* (SA, dark green) and PS treatment. The results are shown as fold change ± SD on the signal of the not treated condition (Ctrl: red dotted line). In both graphs, statistically significant differences between samples and Ctrl are shown by a star.

samples, PS did not cause significant effects, if not for an upregulation of IL-8 and slight downregulation of VEGF, but what was noticed in infected samples was different. With respect to the control, a wound infected by *E. coli* and treated with PS presented an enhanced cell signaling, from the antimicrobial peptide to the cytokine and VEGF expression. *S. aureus*, on the contrary, did not cause the same effects during the antibiotic treatment: the reported genes were downregulated, or differences with the control were not observed. *E. coli*, a Gram-negative bacterium, is known to release endotoxins during its death,[65] also when it is caused by antibiotics.[66,67] Endotoxins are a type of toxin that are associated with the outer layer of the cell membrane of Gram-negative bacteria. They are lipopolysaccharides and are released primarily when the bacteria die as their membrane disintegrates. They are known to be pyrogenic and inflammatory and can led to delayed wound healing, but also necrosis.[65] Thus, as *E. coli* death was witnessed during PS treatment (Figure 6f), the differences in cellular signaling could be due to the different toxins produced by the two bacterial strains during their death. This evidence is crucial, highlighting that developing therapies that only aim for bacterial death is inadequate and can be also harmful but is important to monitor skin reaction during all phases, also after the treatment, to avoid dangerous side effects, as in this case.

https://doi.org/10.1021/acsami.4c16397
ACS Appl. Mater. Interfaces 2024, 16, 70284−70296

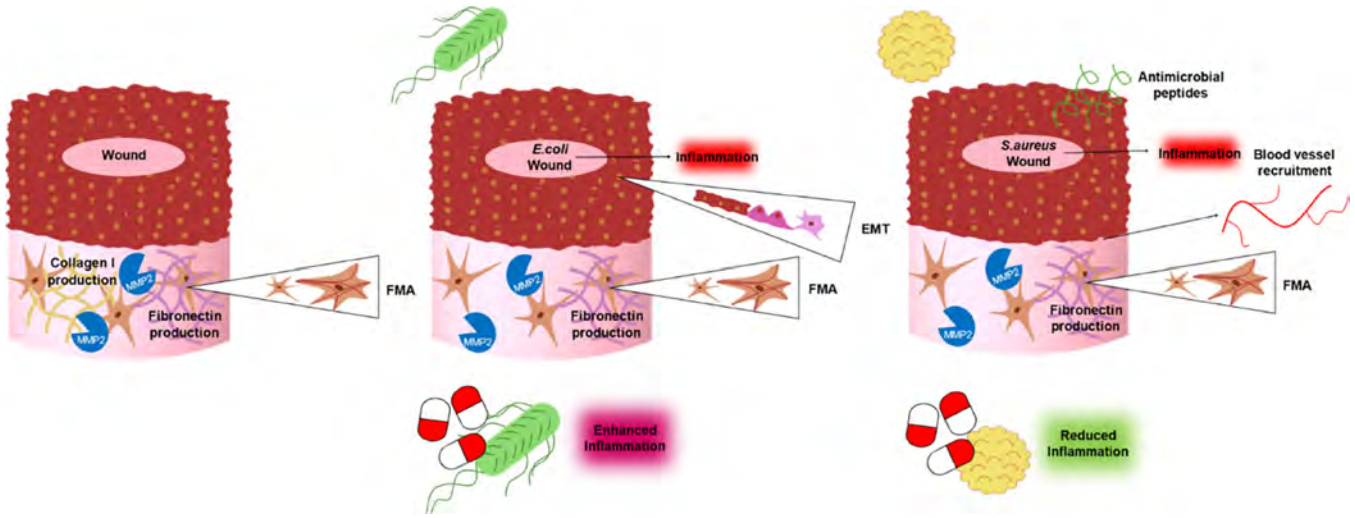

Figure 8. Conclusive scheme of skin model reaction to wounding, infection, and treatment in terms of cellular behavior and signaling.

In Figure 8, it is possible to observe a comprehensive scheme of all the ddPCR analysis conducted on the wounded, infected, and treated skin models, detailed and explained in the previous subparagraphs.

CONCLUSIONS

In vitro skin models are nowadays a powerful tool to investigate the antibacterial efficacy of new and alternative therapies and to study infection progression. The presented dermis–epidermis model was the result of the will to standardize this type of technology and to make it available to as many laboratories as possible, worldwide. For this reason, there were selected two well-known cell lines (HaCaT and HFF-1) and a widely used material, which can be synthesized at low costs (i.e., GelMA). The first evaluation of the model, in terms of physical barrier and fibroblast elongation, was already really promising, witnessing the development of an *in vitro* 3D skin model that can resemble many *in vivo* properties. The following experiments with both *S. aureus* and *E. coli* revealed even more: from one side, they helped to validate the barrier effect, as both after 24 and 48 h after the bacterial inoculation, they were not able to penetrate the epidermal barrier. Moreover, during the controlled infection, the unwounded sample exhibited a lower bacterial proliferation than the wounded counterpart. From the other side, the samples showed a response to wounding and infection that was complex and complete from different points of view. The analyzed behaviors were extracellular matrix deposition and remodeling, inflammatory response and blood vessel recruitment attempt, antimicrobial peptide production, and change in cellular behaviors, from epithelial to mesenchymal (EMT) and from fibroblasts to myofibroblasts (FMA). Interestingly, the skin model reacted in different ways depending on the type of infection: Simple wounding caused the activation of extracellular matrix deposition and remodeling and FMA, while the presence of bacteria led to more complex responses. Both bacterial strains led to high inflammation levels, even with the activation of different cytokines, and to an impairment in extracellular matrix deposition, biased toward FN1 upregulation. *E. coli* was also able to cause EMT, while *S. aureus* enhanced the expression of VEGF and antimicrobial peptides. Basically, the presented *in vitro* skin model showed a performant barrier effect and a complex response to wounds that can be impaired or modified in different ways with the influence of different bacteria.

Another impressive result was that the skin model was able to stand the antibacterial effect of PS, here chosen as a proof-of-concept and validation drug, but the death of the two bacterial strains led to opposite reactions: *S. aureus* death caused a milder inflammatory response and many cellular signals were downregulated, while *E. coli* death led to a stronger inflammation and cellular signaling in general, suggesting the release of endotoxins from the membrane of the dead bacteria. This evidence is essential because it highlights that therapies that focus on killing bacteria are inadequate and can even be harmful. On the contrary, it is crucial to monitor the skin's reaction throughout all phases, including after treatment, to prevent potentially dangerous side effects, as happened in this case.

To conclude, the presented 3D *in vitro* skin model demonstrated the ability to behave in a complex and complete way despite being easily reproducible and low cost. These properties put it in a prominent position for future standardization of platforms to test antibacterial therapies and strategies. To completely take advantage of the 3D *in vitro* skin model response to infection, future studies will explore the integration of vascular components and immune cells. It was indeed demonstrated that the presented model was trying to communicate with both the immune system and the blood vessels during the infection, and understanding how this communication would affect a more complex system is of great interest.

ASSOCIATED CONTENT

Data Availability Statement

The data that support the findings of this work are available within the manuscript.

Supporting Information

The Supporting Information is available free of charge at https://pubs.acs.org/doi/10.1021/acsami.4c16397.

Additional experimental details concerning gene expression analysis and behavior respect to PS treatment (PDF)

https://doi.org/10.1021/acsami.4c16397
ACS Appl. Mater. Interfaces 2024, 16, 70284−70296

AUTHOR INFORMATION

Corresponding Author

Francesca Frascella − *Dipartimento di Scienza Applicata e Tecnologia, PolitoBIOMed Lab, Politecnico di Torino, Turin 10129, Italy;* orcid.org/0000-0002-6543-6038; Email: francesca.frascella@polito.it

Authors

Simona Villata − *Dipartimento di Scienza Applicata e Tecnologia, PolitoBIOMed Lab, Politecnico di Torino, Turin 10129, Italy;* orcid.org/0000-0003-2575-7272

Désirée Baruffaldi − *Dipartimento di Scienza Applicata e Tecnologia, PolitoBIOMed Lab, Politecnico di Torino, Turin 10129, Italy;* orcid.org/0000-0001-8620-9988

Raquel Cue Lopez − *Dipartimento di Scienza Applicata e Tecnologia, PolitoBIOMed Lab, Politecnico di Torino, Turin 10129, Italy*

Camilla Paoletti − *Dipartimento di Ingegneria Meccanica e Aerospaziale, Politecnico di Torino, Turin 10129, Italy*

Paula Bosch − *Departamento de Química Macromolecular Aplicada, Instituto de Ciencia y Tecnología de Polímeros, Consejo Superior de Investigaciones Científicas (CSIC), Madrid 28006, Spain*

Lucia Napione − *Dipartimento di Scienza Applicata e Tecnologia, PolitoBIOMed Lab, Politecnico di Torino, Turin 10129, Italy*

Andrea M. Giovannozzi − *Quantum Metrology and Nano Technologies Division, National Institute of Metrological Research, Turin 10135, Italy*

Candido Fabrizio Pirri − *Dipartimento di Scienza Applicata e Tecnologia, PolitoBIOMed Lab, Politecnico di Torino, Turin 10129, Italy; Center for Sustainable Futures, Istituto Italiano di Tecnologia, Turin 10144, Italy*

Enrique Martinez-Campos − *Departamento de Química Macromolecular Aplicada, Instituto de Ciencia y Tecnología de Polímeros, Consejo Superior de Investigaciones Científicas (CSIC), Madrid 28006, Spain; Grupo de Síntesis Orgánica y Bioevaluación, Instituto Pluridisciplinar (UCM), Madrid 28040, Spain;* orcid.org/0000-0002-7110-3651

Complete contact information is available at: https://pubs.acs.org/10.1021/acsami.4c16397

Notes

The authors declare no competing financial interest.

REFERENCES

(1) Niehues, H.; Bouwstra, J. A.; El Ghalbzouri, A.; Brandner, J. M.; Zeeuwen, P. L. J. M.; van den Bogaard, E. H. 3D Skin Models for 3R Research: The Potential of 3D Reconstructed Skin Models to Study Skin Barrier Function. *Exp. Dermatol.* **2018**, 501−511.

(2) Kang, M. S.; Jang, J.; Jo, H. J.; Kim, W. H.; Kim, B.; Chun, H. J.; Lim, D.; Han, D. W. Advances and Innovations of 3D Bioprinting Skin. *Biomolecules.* **2023**, *13*, 55.

(3) Ponmozhi, J.; Dhinakaran, S.; Varga-Medveczky, Z.; Fónagy, K.; Bors, L. A.; Iván, K.; Erdő, F. Development of Skin-on-a-chip Platforms for Different Utilizations: Factors to Be Considered. *Micromachines.* **2021**, 294−25.

(4) Sutterby, E.; Thurgood, P.; Baratchi, S.; Khoshmanesh, K.; Pirogova, E.Microfluidic Skin-on-a-Chip Models: Toward Biomimetic Artificial Skin. *Small*; Wiley-VCH: Verlag,October 1, 2020, .

(5) Wang, H.; Brown, P. C.; Chow, E. C. Y.; Ewart, L.; Ferguson, S. S.; Fitzpatrick, S.; Freedman, B. S.; Guo, G. L.; Hedrich, W.; Heyward, S.; Hickman, J.; Isoherranen, N.; Li, A. P.; Liu, Q.; Mumenthaler, S. M.; Polli, J.; Proctor, W. R.; Ribeiro, A.; Wang, J.; Wange, R. L.; Huang, S. 3D Cell Culture Models: Drug Pharmacokinetics, Safety Assessment, and Regulatory Consideration. *Clin Transl Sci.* **2021**, *14* (5), 1659−1680.

(6) Kim, B. S.; Gao, G.; Kim, J. Y.; Cho, D. W. 3D Cell Printing of Perfusable Vascularized Human Skin Equivalent Composed of Epidermis, Dermis, and Hypodermis for Better Structural Recapitulation of Native Skin. *Adv. Healthc Mater.* **2019**, *8* (7), No. 1801019.

(7) Zimoch, J.; Zielinska, D.; Michalak-Micka, K.; Rütsche, D.; Böni, R.; Biedermann, T.; Klar, A. S. Bio-Engineering a Prevascularized Human Tri-Layered Skin Substitute Containing a Hypodermis. *Acta Biomater* **2021**, *134*, 215−227.

(8) Lim, K. M. Skin Epidermis and Barrier Function. *Int. J. Mol. Sci.* **2021**, 1−3.

(9) VI The Skin of Mammals.

(10) Kober, J.; Gugerell, A.; Schmid, M.; Kamolz, L. P.; Keck, M. Generation of a Fibrin Based Three-Layered Skin Substitute. *Biomed Res. Int.* **2015**, *2015*, 1.

(11) Wang, Y.; Zhang, H.; Zhou, M.; Yi, X.; Duan, P.; Yu, A.; Qi, B. Autologous Fat Grafting Promotes Macrophage Infiltration to Increase Secretion of Growth Factors and Revascularization, Thereby Treating Diabetic Rat Skin Defect. *Diabetes, Metabolic Syndrome and Obesity* **2020**, *13*, 4897−4908.

(12) Ahn, M.; Cho, W. W.; Lee, H.; Park, W.; Lee, S. H.; Back, J. W.; Gao, Q.; Gao, G.; Cho, D. W.; Kim, B. S. Engineering of Uniform Epidermal Layers via Sacrificial Gelatin Bioink-Assisted 3D Extrusion Bioprinting of Skin. *Adv. Healthc Mater.* **2023**, *12* (27), No. 2301015.

(13) Quan, T.; Wang, F.; Shao, Y.; Rittié, L.; Xia, W.; Orringer, J. S.; Voorhees, J. J.; Fisher, G. J. Enhancing Structural Support of the Dermal Microenvironment Activates Fibroblasts, Endothelial Cells, and Keratinocytes in Aged Human Skin in Vivo. *Journal of Investigative Dermatology* **2013**, *133* (3), 658−667.

(14) Rhee, S. Fibroblasts in Three Dimensional Matrices: Cell Migration and Matrix Remodeling. *Exp. Mol. Med.* **2009**, 858−865.

(15) He, J.; Sun, Y.; Gao, Q.; He, C.; Yao, K.; Wang, T.; Xie, M.; Yu, K.; Nie, J.; Chen, Y.; He, Y. Gelatin Methacryloyl Hydrogel, from Standardization, Performance, to Biomedical Application. *Adv. Healthc Mater.* **2023**, *12* (23), No. 2300395.

(16) Villata, S.; Canta, M.; Baruffaldi, D.; Roppolo, I.; Pirri, C. F.; Frascella, F. 3D Bioprinted GelMA Platform for the Production of Lung Tumor Spheroids. *Bioprinting* **2023**, *36*, No. e00310.

(17) Villata, S.; Frascella, F.; Gaglio, C. G.; Nastasi, G.; Petretta, M.; Pirri, C. F.; Baruffaldi, D. Self-standing Gelatin- Methacryloyl < scp > 3D</Scp> Structure Using < scp > Carbopol</Scp> -embedded Printing. *J. Polym. Sci.* **2024**, *62* (11), 2259−2269.

(18) Gaglio, C. G.; Baruffaldi, D.; Pirri, C. F.; Napione, L.; Frascella, F. GelMA Synthesis and Sources Comparison for 3D Multimaterial Bioprinting. *Front Bioeng Biotechnol* **2024**, *12*, No. 1383010.

(19) Baruffaldi, D.; Palmara, G.; Pirri, C.; Frascella, F. 3D Cell Culture: Recent Development in Materials with Tunable Stiffness. *ACS Appl. Bio Mater.* **2021**, *4* (3), 2233−2250.

(20) Serra, R.; Grande, R.; Butrico, L.; Rossi, A.; Settimio, U. F.; Caroleo, B.; Amato, B.; Gallelli, L.; De Franciscis, S. Chronic Wound Infections: The Role of Pseudomonas Aeruginosa and Staphylococcus Aureus. *Expert Rev. Anti-Infect. Ther.* **2015**, 605−613.

(21) Clebak, K. T.; Malone, M. A. Skin Infections. *Prim. Care* **2018**, 433−454.

(22) Giudice, P. Skin Infections Caused by Staphylococcus Aureus. *Acta Derm. Venereol.* **2020**, *100*, 5725.

(23) Gemeinder, J. L. P.; Barros, N. R. d.; Pegorin, G. S.; Singulani, J. d. L.; Borges, F. A.; Arco, M. C. G. D.; Giannini, M. J. S. M.; Almeida, A. M. F.; Salvador, S. L. d. S.; Herculano, R. D. Gentamicin Encapsulated within a Biopolymer for the Treatment of Staphylococcus Aureus and Escherichia Coli Infected Skin Ulcers. *J. Biomater Sci. Polym. Ed* **2021**, *32* (1), 93−111.

(24) Bessa, L. J.; Fazii, P.; Di Giulio, M.; Cellini, L. Bacterial Isolates from Infected Wounds and Their Antibiotic Susceptibility Pattern: Some Remarks about Wound Infection. *Int. Wound J.* **2015**, *12* (1), 47−52.

(25) Caselli, L.; Malmsten, M. Skin and Wound Delivery Systems for Antimicrobial Peptides. *Curr. Opin. Colloid Interface Sci.* **2023**, No. 101701.
(26) Shah, R. A.; Hsu, J. I.; Patel, R. R.; Mui, U. N.; Tyring, S. K. Antibiotic Resistance in Dermatology: The Scope of the Problem and Strategies to Address It. *J. Am. Acad. Dermatol.* **2022**, 1337−1345.
(27) Wang, C. H.; Hsieh, Y. H.; Powers, Z. M.; Kao, C. Y. Defeating Antibiotic-Resistant Bacteria: Exploring Alternative Therapies for a Post-Antibiotic Era. *International Journal of Molecular Sciences* **2020**, *21*, 1061.
(28) Chang, R. Y. K.; Nang, S. C.; Chan, H. K.; Li, J. Novel Antimicrobial Agents for Combating Antibiotic-Resistant Bacteria. *Adv. Drug Delivery Rev.* **2022**, No. 114378.
(29) Smith, R.; Russo, J.; Fiegel, J.; Brogden, N. Antibiotic Delivery Strategies to Treat Skin Infections When Innate Antimicrobial Defense Fails. *Antibiotics* **2020**, *9*, 56.
(30) Cometta, S.; Hutmacher, D. W.; Chai, L. In Vitro Models for Studying Implant-Associated Biofilms - A Review from the Perspective of Bioengineering 3D Microenvironments. *Biomaterials* **2024**, No. 122578.
(31) Kohda, K.; Li, X.; Soga, N.; Nagura, R.; Duerna, T.; Nakajima, S.; Nakagawa, I.; Ito, M.; Ikeuchi, A. An In Vitro Mixed Infection Model With Commensal and Pathogenic Staphylococci for the Exploration of Interspecific Interactions and Their Impacts on Skin Physiology. *Front Cell Infect Microbiol* **2021**, *11*, No. 712360.
(32) Wiegand, C.; Fink, S.; Mogrovejo, D. C.; Ruhlandt, M.; Wiencke, V.; Eberlein, T.; Brill, F. H. H.; Tittelbach, J. A Standardized Wound Infection Model for Antimicrobial Testing of Wound Dressings in Vitro. *Int. Wound J.* **2024**, *21* (3), No. e14811.
(33) Ventress, J. K.; Partridge, L. J.; Read, R. C.; Cozens, D.; MacNeil, S.; Monk, P. N. Peptides from Tetraspanin CD9 Are Potent Inhibitors of Staphylococcus Aureus Adherence to Keratinocytes. *PLoS One* **2016**, *11* (7), No. e0160387.
(34) Zheng, K.; Balasubramanian, P.; Paterson, T. E.; Stein, R.; MacNeil, S.; Fiorilli, S.; Vitale-Brovarone, C.; Shepherd, J.; Boccaccini, A. R. Ag Modified Mesoporous Bioactive Glass Nanoparticles for Enhanced Antibacterial Activity in 3D Infected Skin Model. *Materials Science and Engineering C* **2019**, *103*, No. 109764.
(35) Shepherd, J.; Sarker, P.; Rimmer, S.; Swanson, L.; MacNeil, S.; Douglas, I. Hyperbranched Poly(NIPAM) Polymers Modified with Antibiotics for the Reduction of Bacterial Burden in Infected Human Tissue Engineered Skin. *Biomaterials* **2011**, *32* (1), 258−267.
(36) Tamer, T. M.; Sabet, M. M.; Omer, A. M.; Abbas, E.; Eid, A. I.; Mohy-Eldin, M. S.; Hassan, M. A. Hemostatic and Antibacterial PVA/Kaolin Composite Sponges Loaded with Penicillin−Streptomycin for Wound Dressing Applications. *Sci. Rep* **2021**, *11* (1), 3428.
(37) Al Kindi, A.; Alkahtani, A. M.; Nalubega, M.; El-Chami, C.; O'neill, C.; Arkwright, P. D.; Pennock, J. L. Staphylococcus Aureus Internalized by Skin Keratinocytes Evade Antibiotic Killing. *Front Microbiol* **2019**, *10* (SEP), 2242.
(38) Van Den Bulcke, A. I.; Bogdanov, B.; De Rooze, N.; Schacht, E. H.; Cornelissen, M.; Berghmans, H. Structural and Rheological Properties of Methacrylamide Modified Gelatin Hydrogels. *Biomacromolecules* **2000**, *1* (1), 31−38.
(39) Kumar, A.; Jagannathan, N. Cytokeratin: A Review on Current Concepts. *International Journal of Orofacial Biology* **2018**, *2* (1), 6.
(40) Kim, Y.; Lim, K. M. Skin Barrier Dysfunction and Filaggrin. *Archives Pharm. Res.* **2021**, 36−48.
(41) van Drongelen, V.; Haisma, E. M.; Out-Luiting, J. J.; Nibbering, P. H.; El Ghalbzouri, A. Reduced Filaggrin Expression Is Accompanied by Increased Staphylococcus Aureus Colonization of Epidermal Skin Models. *Clin. Exp. Allergy* **2014**, *44* (12), 1515−1524.
(42) Levy, L.; Broad, S.; Diekmann, D.; Evans, R. D.; Watt, F. M. Integrins Regulate Keratinocyte Adhesion and Differentiation by Distinct Mechanisms. *Mol. Biol. Cell* **2000**, *11*, 413.
(43) Zhao, X.; Lang, Q.; Yildirimer, L.; Lin, Z. Y.; Cui, W.; Annabi, N.; Ng, K. W.; Dokmeci, M. R.; Ghaemmaghami, A. M.; Khademhosseini, A. Photocrosslinkable Gelatin Hydrogel for Epidermal Tissue Engineering. *Adv. Healthc Mater.* **2016**, *5* (1), 108−118.
(44) Lintzeri, D. A.; Karimian, N.; Blume-Peytavi, U.; Kottner, J. Epidermal Thickness in Healthy Humans: A Systematic Review and Meta-Analysis. *J. Eur. Acad. Dermatol. Venereol.* **2022**, 1191−1200.
(45) Oltulu, P.; Ince, B.; Kokbudak, N.; Findik, S.; Kilinc, F. Measurement of Epidermis, Dermis, and Total Skin Thicknesses from Six Different Body Regions with a New Ethical Histometric Technique. *Turk. J. Plastic Surg.* **2018**, *26* (2), 56−61.
(46) Patten, J.; Wang, K. fibronectin in Development and Wound Healing. *Adv. Drug Delivery Rev.* **2021**, 353−368.
(47) Lenselink, E. A. Role of fibronectin in Normal Wound Healing. *Int. Wound J.* **2015**, *12* (3), 313−316.
(48) Mathew-Steiner, S. S.; Roy, S.; Sen, C. K. Collagen in Wound Healing. *Bioengineering* **2021**, *8*, 63.
(49) Martinez-Garcia, F. D.; van Dongen, J. A.; Burgess, J. K.; Harmsen, M. C. Matrix Metalloproteases from Adipose Tissue-Derived Stromal Cells Are Spatiotemporally Regulated by Hydrogel Mechanics in a 3D Microenvironment. *Bioengineering* **2022**, *9* (8), 340.
(50) Kandhwal, M.; Behl, T.; Singh, S.; Sharma, N.; Arora, S.; Bhatia, S.; Al-Harrasi, A.; Sachdeva, M.; Bungau, S.*Role of Matrix Metalloproteinase in Wound Healing*; **2022**; Vol. *14*. www.ajtr.org.
(51) Shie, M. Y.; Lee, J. J.; Ho, C. C.; Yen, S. Y.; Ng, H. Y.; Chen, Y. W. Effects of Gelatin Methacrylate Bio-Ink Concentration on Mechano-Physical Properties and Human Dermal Fibroblast Behavior. *Polymers (Basel)* **2020**, *12* (9), 1930.
(52) Pfisterer, K.; Shaw, L. E.; Symmank, D.; Weninger, W. The Extracellular Matrix in Skin Inflammation and Infection. *Front. in Cell Dev. Biol* **2021**, No. 682414.
(53) Gimeno-Lluch, I.; Benito-Jardón, M.; Guerrero-Barberà, G.; Burday, N.; Costell, M. The Role of the fibronectin Synergy Site for SkinWound Healing. *Cells* **2022**, *11* (13), 2100.
(54) Huang, J.; Heng, S.; Zhang, W.; Liu, Y.; Xia, T.; Ji, C.; Zhang, L. J. Dermal Extracellular Matrix Molecules in Skin Development, Homeostasis, Wound Regeneration and Diseases. *Semin. Cell Dev. Biol.* **2022**, 137−144.
(55) Stone, R. C.; Pastar, I.; Ojeh, N.; Chen, V.; Liu, S.; Garzon, K. I.; Tomic-Canic, M. Epithelial-Mesenchymal Transition in Tissue Repair and Fibrosis. *Cell Tissue Res.* **2016**, 495−506.
(56) Haensel, D.; Dai, X. Epithelial-to-Mesenchymal Transition in Cutaneous Wound Healing: Where We Are and Where We Are Heading Cutaneous Wound Healing. *Dev. Dyn.* **2018**, *247*, 473−480.
(57) Li, M.; Luan, F.; Zhao, Y.; Hao, H.; Zhou, Y.; Han, W.; Fu, X. Epithelial-Mesenchymal Transition: An Emerging Target in Tissue Fibrosis. *Exp Biol. Med.* **2016**, *241* (1), 1−13.
(58) Piipponen, M.; Li, D.; Landén, N. X. The Immune Functions of Keratinocytes in Skin Wound Healing. *Int. J. Mol. Sci.* **2020**, 8790.
(59) Herman, A.; Herman, A. P. Antimicrobial Peptides Activity in the Skin. *Skin Res. Technol.* **2019**, 111−117.
(60) Haisma, E. M.; Rietveld, M. H.; Breij, A.; Van Dissel, J. T.; El Ghalbzouri, A.; Nibbering, P. H. Inflammatory and Antimicrobial Responses to Methicillin-Resistant Staphylococcus Aureus in an in Vitro Wound Infection Model. *PLoS One* **2013**, *8* (12), No. e82800.
(61) Ritsu, M.; Kawakami, K.; Kanno, E.; Tanno, H.; Ishii, K.; Imai, Y.; Maruyama, R.; Tachi, M. Critical Role of Tumor Necrosis Factor-α in the Early Process of Wound Healing in Skin. *Journal of Dermatology & Dermatologic Surgery* **2017**, *21* (1), 14−19.
(62) Cavagnero, K. J.; Gallo, R. L. Essential Immune Functions of Fibroblasts in Innate Host Defense. *Front. Immunol.* **2022**, No. 1058862.
(63) Johnson, B. Z.; Stevenson, A. W.; Prêle, C. M.; Fear, M. W.; Wood, F. M. The Role of IL-6 in Skin Fibrosis and Cutaneous Wound Healing. *Biomedicines* **2020**, *8* (5), 101.
(64) Johnson, K. E.; Wilgus, T. A. Vascular Endothelial Growth Factor and Angiogenesis in the Regulation of Cutaneous Wound Repair. *Adv. Wound Care (New Rochelle)* **2014**, *3* (10), 647−661.
(65) Cavaillon, J. M. Exotoxins and Endotoxins: Inducers of Inflammatory Cytokines. *Toxicon* **2018**, 45−53.

https://doi.org/10.1021/acsami.4c16397
ACS Appl. Mater. Interfaces 2024, 16, 70284−70296

(66) Dofferhoff, A. S. M.; De Vries-Hospers, H. G.; Zanten, A. V.; Bom, V. J. J.; Weits', J.; Vellenga, E. Release of Endotoxin from Antibiotic-Treated Escherichia Coli and the Production of Tumour Necrosis Factor by Human Monocytes. *J. Antimicrob. Chemother.* **1993**, *31*, 373.
(67) Kirikae, T.; Kirikae, F.; Saito, S.; Tominaga, K.; Tamura, H.; Uemura, Y.; Yokochi, T.; Nakano, M.*Biological Characterization of Endotoxins Released from Antibiotic-Treated Pseudomonas Aeruginosa and Escherichia Coli*; **1998**; Vol. *42*. https://journals.asm.org/journal/aac.

https://doi.org/10.1021/acsami.4c16397
ACS Appl. Mater. Interfaces 2024, 16, 70284−70296